# Dynamics of Chemical and Charge-Transfer Reactions of Molecular Dications: III. Beam Scattering and Total Cross Section Data for Processes in the System $CO_2^{2+} + D_2$

**Libor Mrázek, Jan Žabka, Zdenek Dolejšek, Jan Hrušák, and Zdenek Herman***

*V. Čermák Laboratory, J. Heyrovský Institute of Physical Chemistry, Academy of Sciences of the Czech Republic, Dolejškova 3, CZ-182 23 Prague 8, Czech Republic*

*Received: March 28, 2000; In Final Form: June 1, 2000*

Chemical reactions and charge-transfer processes in the system $CO_2^{2+} + D_2$ were investigated in crossed-beam scattering experiments. Theoretical calculations of stationary points on the dication potential energy surface $(CO_2D_2)^{2+}$ were carried out to complement the experiments. The main ion products identified were $CO_2D^+$, COD, $CO_2^+$, $CO^+$, and $O^+$. The relative cross sections for reactions with $D_2$ ($H_2$) were in the ratio $CO_2^+$:$COD^+$:$CO_2D^+$ = 100:10:1 and were almost independent of the collision energy over the range 0.5−4 eV (center-of-mass, C.M.). The chemical product $CO_2D^+$ was formed in a nondissociative chemical reaction leading to $CO_2D^+ + D^+$ through two channels that released different amounts of translational energy via decomposition of intermediates $(CO_2D_2)^{2+}$; the high translational energy release channel (peak value at 4 eV) is consistent with the energetics of formation of a D−C-bonded isomer $DCO_2^+$, which dissociates further to form $DCO^+ + O$. The charge-transfer product $CO_2^+$ is formed prevailingly in the excited states A and B; a small amount is also formed by further dissociation of the product $CO_2D^+$ (formed in the low translational energy release channel, presumably in an excited state) to $CO_2^+ + D$. The product $CO^+$ results from two different processes: from charge transfer leading to $CO_2^+(C^2\Sigma_g^+) + D_2^+$ and predissociation of the C state to $CO^+(X^2\Sigma^+) + O(^3P)$ and from spontaneous dissociation of the projectile $CO_2^{2+}$ (vibrationally excited to its predissociation barrier) to $CO^+ + O^+$.

## 1. Introduction

Chemical reactions of doubly charged ions (dications) with neutral species represent a new and exciting class of elementary chemical processes.[1−6] Because of the high energy content of dications (30−40 eV above the respective neutrals), their reactions often lead to the creation of electronically excited species, the subsequent decomposition of internally excited products, and the formation of pairs of singly charged ions with large relative translational energy; thus, the energy partitioning in products may differ from that of both cation−neutral or neutral−neutral reactions. Also, formation of "naked" fast protons[2−5] in reactions of molecular dications with hydrogen is yet another rather unusual feature of these processes. Chemical reactions of dications usually occur in strong competition with charge-transfer processes that lead to the formation of two singly charged products

$$A^{2+} + BC \rightarrow A^+ + BC^+ \qquad (1)$$

A large amount of data has been obtained on the cross section and energy partitioning of these electron-exchange processes.[3,7,8]

Chemical reactions of dications are basically of two types: bond forming reactions between dications and neutrals in which a doubly charged ion product and a neutral particle are formed, such as

$$A^{2+} + BC \rightarrow AB^{2+} + C \qquad (2)$$

or reactions in which two singly charged ions are formed as a result of a bond-rearrangement collision between a dication and a neutral

$$A^{2+} + BC \rightarrow AB^+ + C^+ \qquad (3)$$

The latter type is of particular interest because of the expectedly high translational energy release due to Coulomb repulsion between the products.

In our earlier communications,[3−5] we reported crossed-beam scattering studies of processes in the system $CF_2^{2+} + D_2$. The nondissociative processes of charge transfer (1) and chemical rearrangement leading to the formation of $CF_2D^+$ were shown to be prime examples of these dication−molecule processes, characterized by high translational energy release due to the Coulomb repulsion between the singly charged products. A potential surface model for reactions of dications with molecules was developed that is based on transitions occurring at crossings of the potential energy surfaces of the dication−neutral system with the Coulomb repulsion surfaces of the two singly charged products in the reactant (charge transfer) or product (chemical bond rearrangement) valley. The model accounts for mutual competition of the above-mentioned processes 1−3 in a variety of systems.[5]

In this paper, we describe results of a related crossed-beam scattering study of the system $CO_2^{2+} + D_2$. Earlier mass spectrometric studies of this system[2,10] described formation of the products $CO_2^+$, $CO^+$, $CO_2D^+$, and $COD^+$ and their relative abundances at selected collision energies. It appears that the products are formed in both nondissociative and dissociative charge-transfer processes and chemical-rearrangement reactions, but essentially no further detailed information exists, especially on the mechanisms, energetics, and dynamics of the elementary processes. Our investigation brings new data on the relative total cross sections in collisions with $D_2$ and $H_2$ and their dependence on collision energy. Scattering data on the processes of formation of the above-mentioned products, in combination with the calculated potential energy surface of $[CO_2H_2]^{2+}$, provide

10.1021/jp0011645 CCC: $19.00 
Published on Web 07/15/2000

information that makes it possible to elucidate both the mechanisms and the reaction pathways leading to various products and the dynamics of the respective elementary processes.

## 2. Methods

**2.1. Experiments and Data Treatment.** The experiments were carried out on the crossed-beam apparatus EVA II. The performance and application of this apparatus to this type of scattering experiments was described earlier.[3−5] Briefly, the $CO_2^{2+}$ dications were produced by impact of 130 eV electrons on $CO_2$ in a low-pressure ion source. The ions were extracted, mass analyzed, and decelerated by a multielement lens to the required laboratory energy. The $CO_2^{2+}$ beam was crossed at right angles with a beam of $D_2$ ($H_2$) molecules emerging from a multichannel jet. The ion beam had angular and energy spreads of 1° and 0.3 eV (full-width at half-maximum, fwhm), respectively; the collimated neutral beam had an angular spread of 6° (fwhm) and thermal energy distribution at 300 K. Reactant and product ions passed through a detection slit (2.5 cm from the scattering center) into a stopping-potential energy analyzer. They were then accelerated and focused into the detection mass spectrometer, mass analyzed, and detected with the use of a dynode electron multiplier. Angular distributions were obtained by rotating the two beams about the scattering center. Modulation of the neutral beam and phase-sensitive detection of the ion products were used to remove background scattering effects.

Laboratory angular distributions and energy profiles recorded at 6−10 laboratory scattering angles were used to construct scattering diagrams of the investigated products; the contours in the scattering diagrams refer to the Cartesian probability distribution,[11] normalized to the maximum in the particular scattering diagram. Center-of-mass (C.M.) angular distributions (relative differential cross sections) and relative translational energy distributions of the products were then obtained in the usual way.[11]

In the measurements of the total cross sections, the dependence on the collision energy of the ratio of the product ion and reactant ion intensities, $I_{P,m}/I_{R,m}$, was measured at the ion angular maximum, at a constant pressure of the neutral reactant ($D_2$ or $H_2$). The relative total cross section $\sigma_{rel}$ was then determined as

$$\sigma_{rel} = I_{P,m}/I_{R,m}\,[\int I_P(\Theta)\,d\Theta]/I_{P,m} \qquad (5)$$

The correction factor $[\int I_P(\Theta)\,d\Theta]/I_{P,m}$ is a normalized integral over the laboratory angular distribution of the product. This is, of course, only an approximate correction, as it assumes that the product ions all have the same velocity at a particular collision energy. However, because the scattering diagrams of the products are rather similar, this method turned out to be more accurate than integration of the (absolute) Cartesian probability distribution over the scattering diagram. In any event, the correction factor played only a minor role and could be neglected in comparison with other sources of errors.[6] The scatter in the measured data (Figure 1) comes mainly from difficulties in exactly locking in the phase of the product ion signal for the determination of the ratio of the product ion intensity (modulated ac signal) to the reactant ion intensity (dc signal). The values of the relative total cross sections in Figure 1 are mutually in scale.

In the measurement of the spontaneous dissociation of $CO_2^{2+}$ to $CO^+ + O^+$, energy profiles of the dc ion intensities of $CO^+$ and $O^+$ (not their locked-in components) were determined.

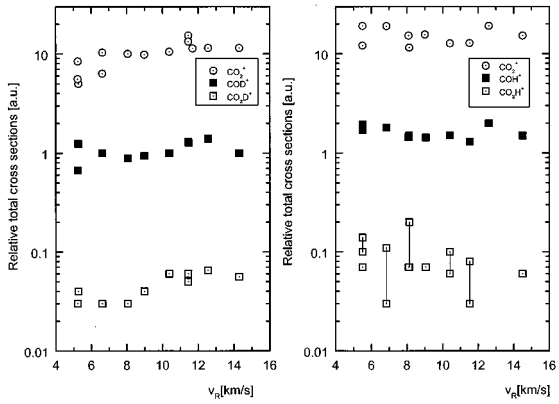


**Figure 1.** Dependence of the relative total cross sections for the formation of $CO_2^+$, $COD^+(COH^+)$, and $CO_2D^+(CO_2H^+)$ in collisions of $CO_2^{2+}$ with $D_2$ ($H_2$) on the relative velocity of the reactants, $v_R$.

**2.2. Calculations.** Calculations of stationary points on the potential energy hypersurface $(CO_2H_2)^{2+}$ were carried out using the Gaussian 98 program.[12] Geometries were fully optimized at the B3LYP/cc-pvTZ level.[13,14] Harmonic frequencies were calculated at each point. The final energies were refined at the coupled-cluster [CCSD(T)] level. Only triplet states relevant to the subject of this paper will be discussed here. The full account of the calculations will be published separately.

**2.3. Energetics of $CO_2^{2+}$.** The double-ionization energy IE-($CO_2 \rightarrow CO_2^{2+}$) is known from photoionization studies.[15] The most recent value[16] is 37.36 eV; hence, the value of 37.4 eV will be used in this paper. An important theoretical paper[17] provides data on potential energy curves of the ground and excited states of $CO_2^{2+}$, their stability and energy barriers for dissociation, and the population of vibrational levels in the double-ionization process. From this work and from charge-transfer translational energy spectroscopy studies between $CO_2^{2+}$ and Ne[18,19] and Ar,[19] one can conclude that both the ground $X^3\Sigma_g^-$ state and the singlet excited states $A^1\Delta_g$ (calculated, in good agreement with experimental results and other calculations,[15] to be 1.35 eV above the ground state) $B^1\Sigma^+_g$ (1.93 eV above the ground state) and $C^1\Sigma_u^-$ (2.55 eV above the ground state) are evidently present in the reactant beam. Relative populations of the ground and excited states could be obtained from photoionization studies, but no data are available at the moment. However, from the charge-transfer behavior, one can approximate that a substantial fraction of the dications are generated in their ground state. From the calculated Franck−Condon factors for double ionization,[17] one can estimate that vibrational excitation of $CO_2^{2+}$, gained in the direct double-ionization process, is not very large: it ranges between 0 and 0.4 eV with a mean value of about 0.2 eV for the above-mentioned electronic states.

The energetics and stability of the low-lying electronic states of the cation $CO_2^+$ are well-known from photoelectron spectroscopy measurements.[20−22] The ground-state $CO_2^+(X^2\Pi_g)$ lies at 13.79 eV, and the lowest stable excited states are $A^2\Pi_u$ and $B^2\Sigma_u^+$, 3.8 and 4.3 eV above it, respectively. The $C^2\Sigma_g^+$ state, 5.6 eV above the ground state, is known to be essentially fully predissociative mostly to the asymptote $CO^+(X^2\Sigma_g^+) + O(^3P)$ lying close to it.[21]

## Results and Discussion

**3.1. Relative Total Cross Sections.** Figure 1 shows the dependence of the relative total cross sections for formation of product ions $CO_2^+$, $COD^+$ ($COH^+$), and $CO_2D^+(CO_2H^+)$ on the relative velocity of the reactants. Cross sections for the

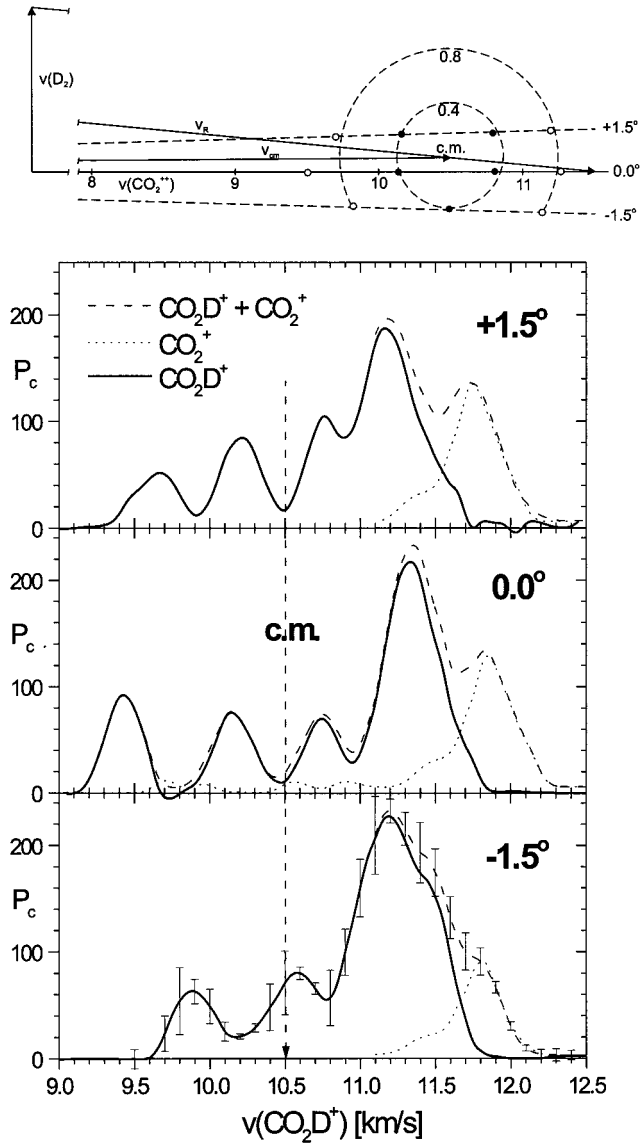


**Figure 2.** Velocity profiles of $CO_2D^+$ from reaction 5 at the laboratory scattering angles of +1.5°, 0.0°, and −1.5°. The dashed lines refer to measured data, and the solid lines are data obtained after subtraction of the isotopic contribution of $^{12}C^{18}O^{16}O^+$ from reaction 4 at the same mass (dotted lines). Vertical error bars with the velocity profile at −1.5° show the standard error of the data averaged from 7 measurements. The Newton diagram in the upper part of the figure shows the locations of the maxima with respect to the center-of-mass (C.M.).

formation of $CO_2D^+$ and $CO_2H^+$ were corrected for isotopic contributions from the $CO_2^+$ product intensity. Processes that give rise to these ions can be identified as (for $D_2$; analogous reactions for collisions with $H_2$)

$$CO_2^{2+} + D_2 \rightarrow CO_2^+ + D_2^+$$
(nondissociative charge transfer) (4)

$$\rightarrow CO_2D^+ + D^+$$
(nondissociative chemical reaction) (5)

$$\rightarrow COD^+ + (D + O)^+$$
(dissociative chemical reaction) (6)

(for energetics of possible processes involved, see below, Figure 11). Formation of $CO^+$ and $O^+$ ions was also observed. However, these ions were formed both by collisions with deuterium (hydrogen) and by spontaneous dissociation of the projectile ion (without collision gas), and thus, the magnitudes of the cross sections were difficult to specify (see below, section 3.2.4). Small amounts of ions $D^+$ and $D_2^+$ could be detected but could not be reliably measured.

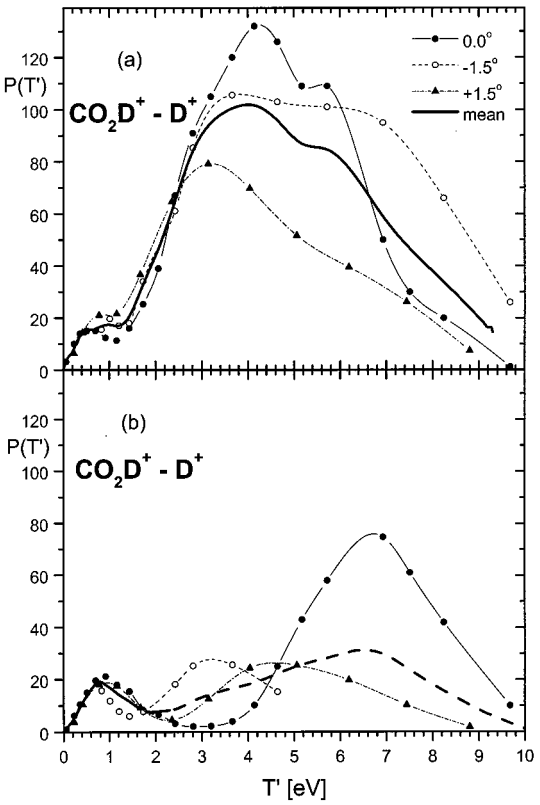


**Figure 3.** Relative translational energy distributions of the products of reaction 5, $P(T')$ vs. $T'$, at the three laboratory scattering angles, as calculated from the data in Figure 2. (a) Forward-scattered product $CO_2D^+$. (b) Backward-scattered product $CO_2D^+$. The solid lines show averages of the three curves.

The cross sections in Figure 1 differ considerably in size: nondissociative charge transfer (eq 4) exhibits the largest cross section. The cross section for the formation of $COD^+$ ($COH^+$) is about an order of magnitude smaller, and that for the formation of $CO_2D^+$ ($CO_2H^+$) is about 2 orders of magnitude smaller than the cross section for the charge-transfer process (eq 4). All cross sections show (within the experimental error) only a slight dependence on the relative velocity of the reactants over the studied region. In the case of nondissociative charge transfer (eq 4), this seems to indicate contributions to the total cross sections of several state-to-state processes of different exoergicities (from several states of the reactant ion to several states of the product ion), which presumably blur and mutually compensate for the dependencies of particular state-to-state cross sections on the relative velocity.[6]

**3.2. Scattering Results.** *3.2.1. Formation of $CO_2D^+$.* Although the total cross section for the formation of this ion is the smallest measured, this nondissociative chemical reaction provides a clue to several dissociative processes, and thus, it will be discussed first. Because of an extremely low intensity, however, the scattering diagrams for $CO_2D^+$ could not be obtained, only energy (velocity) profiles at several scattering angles closest to the angular maximum and at the higher of the two collision energies investigated could be derived from a long series of repeated stopping-potential curve measurements.

Figure 2 shows velocity profiles of $CO_2D^+$ from reaction 2 at the collision energy of 2.5 eV. The profiles were measured

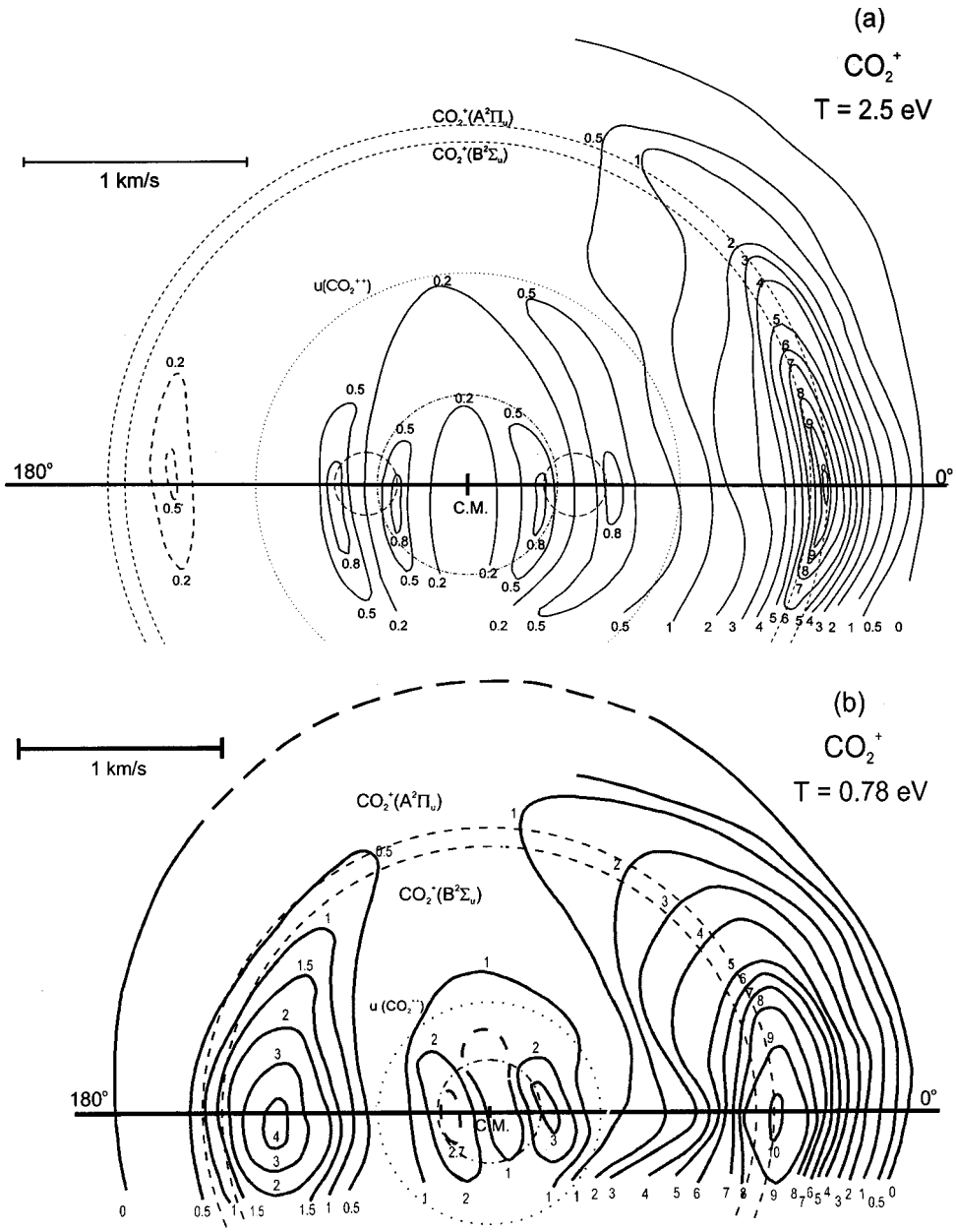


**Figure 4.** Contour scattering diagrams of $CO_2^+$ at collision energies of (a) 2.5 and (b) 0.78 eV. The solid line denotes the direction of the relative velocity vector, and C.M. denotes the position of the tip of the center-of-mass velocity vector. The dotted circle denotes the initial center-of-mass velocity of the reactant $CO_2^{2+}$. The dashed circles show the loci where the product $CO_2^+$ should appear if formed in reaction 4 in the vibrationally ground states of the electronic states indicated. The dash-dotted circles at $u(CO_2^+) = 0.4$ km/s and the two small dashed circles refer to the discussion of $CO_2^+$ formed by dissociation of $CO_2D^+$ (see section 3.2.2).

at the laboratory scattering angles of +1.5°, 0.0°, and −1.5°, and they are averages of 4−7 30-min measurements. In the figures, the dashed lines are the original data, the dotted lines represent subtraction of the isotopic contribution from $C^{18}O^{16}O^+$ of the charge-transfer product from reaction 4 (as determined from the respective velocity profiles in Figure 4a, see below), and the strong solid lines are the velocity distributions of pure $CO_2D^+$. As an example, vertical error bars with the velocity profile at −1.5° show the standard error of the data averaged from 7 measurements. The subtraction practically removes the highest peak and leaves 4 (3 at −1.5°) peaks. The peaks in velocity profiles form two pairs, symmetrically placed (within the experimental error) forward and backward with respect to the position of the center-of-mass (C.M.) of the system (dashed vertical line in Figure 2). The location of the peaks with respect to the C.M. can be well observed in the top part of Figure 2, where the positions of the velocity maxima are shown in the framework of the respective Newton diagram: the inner and outer peaks fall close to circles with $u'(CO_2D^+)$ values of 0.4 and 0.8 km/s, respectively. The only exception is the backward outer maximum at 0.0°, which comes out at about 0.3 km/s lower than expected; this, however, results presumably from an experimental inaccuracy.

The two inner peaks are of about the same height (at −1.5°, they merge into one close to the C.M.). On the other hand, in the pair of outer maxima, the height of the low-velocity backward peak is about 30−50% that of the forward peak. The fully or partly developed forward−backward symmetry suggests that the products of reaction 2, $CO_2D^+ + D^+$, are formed via decomposition of intermediates $[CO_2D_2^{2+}]$ with mean lifetimes of about a picosecond or longer. Figure 3 transforms the velocity profiles of Figure 2 into plots of relative product translational energy, $P(T')$, vs $T'$ for the three scattering angles, separately for the forward (a) and backward (b) scattering. Although the

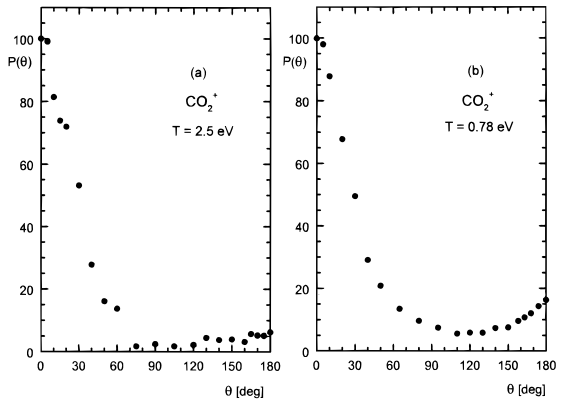


**Figure 5.** C.M. angular distributions (relative differential cross sections) of $CO_2^+$ at collision energies of (a) 2.5 and (b) 0.78 eV.

scatter of the data is appreciable [notably, the outer backward peak at 0.0° leads to unrealistically high $P(T')$ peaking], the following conclusions can be made: (1) The products of nondissociative chemical reaction 5 at the collision energy of 2.5 eV (C.M.) are formed in two processes of different translational energy release via decomposition of intermediates $[CO_2D_2^{2+}]$. (2) The process of low translational energy release (peak value at 0.45 eV) is connected with the decomposition of a complex with a mean lifetime longer than several picoseconds, as implied by the forward−backward symmetry of the scattering (inner peaks in Figure 2). (3) The process of high translational energy release (peak value at about 4.5 eV, a broad distribution of translational energy between about 2 and 9 eV) can be related to the decomposition of an osculating intermediate with a mean lifetime of about a picosecond, as suggested by the asymmetry in the forward−backward scattering (outer peaks in Figure 2).

In the following sections, we will show that the scattering results help to identify the product $CO_2D^+$ as a precursor of secondary dissociation processes in which $COD^+$ and a small amount of $CO_2^+$ is formed.

*3.2.2. Formation of $CO_2^+$.* Scattering diagrams of $CO_2^+$ formed in $CO_2^{2+} + D_2$ encounters at collision energies (C.M.) of 2.5 and 0.78 eV are shown in Figure 4a,b, respectively. In the diagrams, the horizontal solid line shows the direction of the relative velocity vector, and C.M. indicates the position of the tip of the center-of-mass velocity vector. The dotted circle shows the center-of-mass velocity of the reactant dication $CO_2^{2+}$. In the center-of-mass coordinates, the projectile $CO_2^{2+}$ approaches from the left (designated as the C.M. scattering angle 180°), and the neutral reactant $D_2$ approaches from the right.

In both scattering diagrams, the product $CO_2^+$ is scattered preferentially forward with respect to the direction of the incoming projectile $CO_2^{2+}$, with a velocity that considerably exceeds the initial C.M. velocity of the projectile (dotted circle). The ridge of the distribution follows the product velocity loci, where $CO_2^+$ should appear, if formed in the nondissociative charge transfer eq (4) in the excited states $CO_2^+(A^2\Pi_u)$ and $CO_2^+(B^2\Sigma_u)$ (dashed circles in Figure 4a,b). A much smaller (5% at 2.5 eV) peak of backward scattering is located inside the dashed circles, suggesting a somewhat lower translational energy release in the charge-transfer process. In addition, there is a small intensity of the product $CO_2^+$ forming the total of four weak maxima lying inside the dotted circle of the reactant initial velocity $u(CO_2^{2+})$. This is indicative of the product formed in a *translationally endoergic* process, as discussed below in this section.

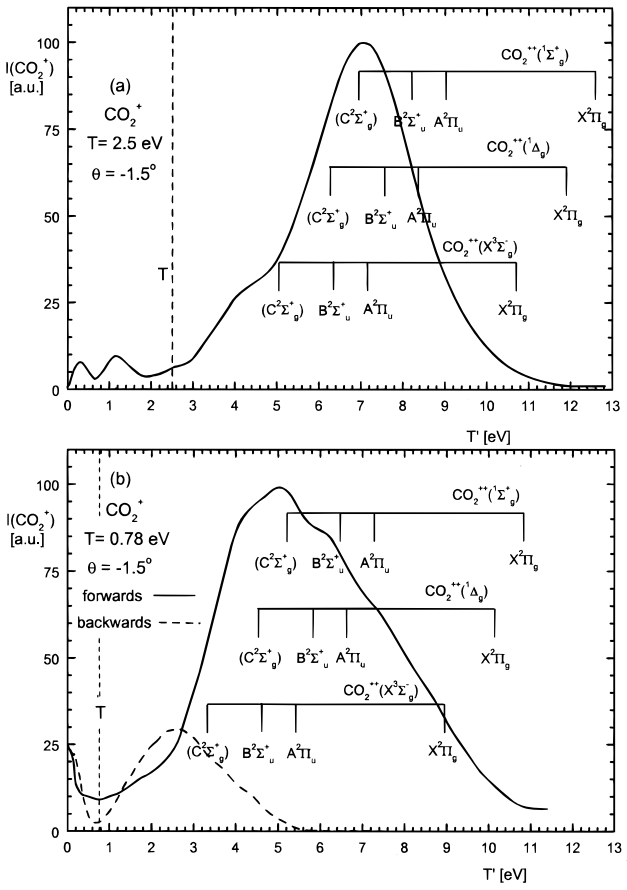


**Figure 6.** Dependence of the intensity profiles of $CO_2^+$, $I(CO_2^+)$, on the product relative translational energy $T'$ at the laboratory scattering angle of −1.5° for the collision energies of (a) 2.5 and (b) 0.78 eV. The vertical dashed line indicates the collision energy $T$. The scales in the figure show product energy thresholds for formation of ground and excited states of $CO_2^+$ in collisions with ground and excited states of the reactant ion $CO_2^{2+}$ (designation above the scales), assuming no internal (vibrational and rotational) excitation of the molecular species.

Figure 5 shows the relative differential cross sections (C.M. angular distributions) of the product $CO_2^+$, as obtained by the integration of the scattering diagrams. As observed earlier for both atomic and molecular charge-transfer systems, the product ion shows a strongly forward-peaked scattering, which is in general agreement with the existing models.[3,23]

Figures 6 and 7 summarize data on the translational energy of the charge-transfer products from reaction 4 at the collision energies 2.5 and 0.78 eV, respectively. Figure 6 brings energy profiles of $CO_2^+$ measured at the laboratory scattering angle of −1.5° (close to the angular maximum) forward with respect to the position of the C.M. The profiles are plotted with respect to the product relative translational energy $T'$ ($T' = T + \Delta E$, where $T$ is the relative translational energy of the reactants and $\Delta E$ is the exoergicity of the process). The scales in the figure indicate $T'$ for the exoergicities of processes from specific electronic states of the reactant ion to specific electronic states of product ion; the vertical dashed line gives $T$. Figure 7 shows the $P(T')$ curves at the two collision energies obtained by the integration over the entire scattering diagrams, plotted as usual with respect to the product relative translational energy $T'$ (again, $T$ is shown by the vertical dashed line). The energy profiles at −1.5° exhibit an intrinsically better energy resolution than the $P(T')$ curves, which integrate in all inaccuracies of the scattering diagrams. Despite the unresolved, overlapping character of the curves in Figures 6 and 7, they can be understood in the

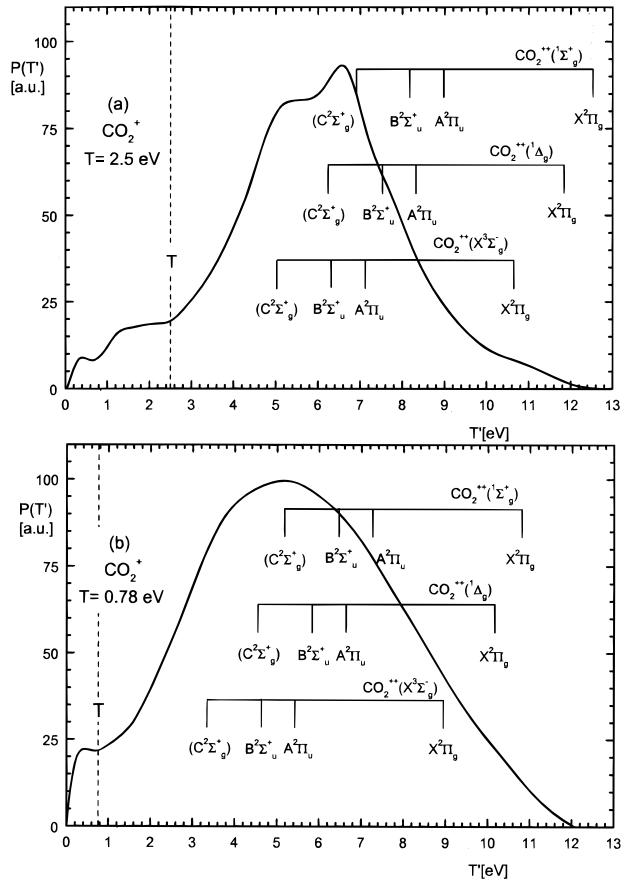


**Figure 7.** Relative translational energy distribution curves, $P(T') - T'$, of products $CO_2^+ + D_2^+$ at the collision energies of (a) 2.5 and (b) 0.78 eV. Other designations are the same as in Figure 6a,b.

following way: the scales with state designation in the figures refer to translational energy release in the limiting transitions from the vibrational ground state of the reactant ion to the vibrational ground states of the products. Higher energy release (to the right of the vertical lines) indicates participation of the vibrationally excited reactant ion ("hot bands"). This contribution, however, may be expected to be rather small, below about 0.4 eV (see section 2.3). Vibrational excitation of the product ions (either $CO_2^+$ or also $D_2^+$) shifts the energy release to lower than limiting values (to the left of the corresponding vertical lines). Thus, all energy profiles show that the main portion of the product $CO_2^+$ is formed in exoergic processes of nondissociative charge transfer (reaction 4), leading preferentially to the excited states $CO_2^+(A^2\Pi)$ and $CO_2^+(B^2\Sigma_u)$. The distributions clearly indicate participation of both the ground and, to a certain extent, the excited states of the projectile dication $CO_2^{2+}$ in reaction 4 and formation of the product $CO_2^+$ in the A and B states with some amount of internal (vibrational) excitation. Formation of the $CO_2^+(C^2\Sigma^+_g)$ state is unlikely, as this state is known to be essentially fully predissociative[9,21] (see also the section on $CO^+$ formation).

The scattering diagrams of $CO_2^+$ in Figure 4 also reveal formation of a small amount of the product $CO_2^+$ close to the C.M., within the dashed circle that denotes the initial C.M. velocity of the ion reactant, $u(CO_2^{2+})$. In the $P(T')$ distributions in Figure 7, this gives rise to the weak maxima at low $T'$ (0.4 and 1.4 eV for 2.5 eV and 0.3 eV for 0.78 eV). The product comes from *translationally endoergic* processes; thus, its formation cannot be explained by the Landau−Zener formalism of potential surface crossing that underlines the formation of most of the product in exoergic processes of nondissociative charge transfer, reaction 4. A closer inspection of the scattering diagram in Figure 4a shows that this low-energy product is concentrated in two pairs of ridges of equal intensity forward and backward from the C.M.; the minima between the ridges fit very well on a circle of $u(CO_2^+) = 0.4$ km/s (dashed curve in Figure 4a), where the two inner maxima of the chemical product $CO_2D^+$ occur (see Figure 2). This strongly suggests that the product $CO_2^+$ in this region of the scattering diagram results from further dissociation of the chemical product $CO_2D^+$ described by

$$CO_2^{2+} + D_2 \rightarrow [CO_2D_2]^{2+} \rightarrow (D^+) + CO_2D^+ \rightarrow CO_2^+ + D \quad (7)$$

The mean energy of the dissociating pair $CO_2^+ + D$ can be obtained from the separation of the two ridges of a pair (dash-dotted circles in Figure 4a), and it is found to be—in the vicinity of the relative velocity line—0.3 km/s; this leads to the mean relative translational energy of the dissociating pair of about 0.15 eV. The situation at the collision energy of 0.78 eV is analogous (Figure 4b). However, the two pairs of peaks close to the C.M. in Figure 4a collapse into one pair in Figure 4b, forward and backward from the C.M. This is because, at this lower collision energy, the two inner maxima in the velocity profiles of $CO_2D^+$ may be expected to shrink into one peak located at the C.M. The separation between the peaks, 0.45 km/s, leads to an average relative translational energy for the dissociating pair of about 0.25 eV.

The ratio of the cross sections of forming the product $CO_2^+$ by dissociation of $CO_2D^+$ and by charge-transfer process 4 can be roughly estimated from Figure 7a,b. As the $P(T')$ curves are obtained by a 3D integration of the scattering diagrams,[11] the area under the curve is proportional to the total cross section, and its respective parts directly reflect the ratios of the total cross sections pertinent to the respective processes. Thus, if one compares the areas of the endoergic and exoergic parts under the $P(T')$ curves in Figure 7a,b, one can estimate that, of the total amount of $CO_2^+$ formed, about 4% originates from the dissociation of $CO_2D^+$ at the collision energy of 2.5 eV, and about 2% at the collision energy of 0.78 eV.

*3.2.3. Formation of COD*$^+$. The reaction product $COD^+$ is obviously a product of a dissociative chemical reaction. The mechanism of its formation can be understood by analyzing the scattering diagrams of $COD^+$, as shown in Figure 8a,b for the collision energies of 2.5 and 0.85 eV, respectively. The diagrams show distributions with four peaks grouped in pairs forward and backward with respect to the C.M. At 2.5 eV, the minima between the peaks of both the forward and backward pairs lie on a circle of radius of 0.8 km/s, which is, within the experimental error, the same as the separation from the C.M. of the outer maxima of the $CO_2D^+$ profiles in Figure 2. Thus the peaks of $CO_2D^+$ lie *between* the peaks of $COD^+$. This suggests that the product $COD^+$ is formed by further decomposition to $COD^+ + O$ of the primary chemical product $CO_2D^+$ formed in the high translational energy release process (see section 3.2.1), i.e., in the reaction sequence

$$CO_2^{2+} + D_2 \rightarrow [CO_2D_2]^{2+} \rightarrow (D^+) + CO_2D^+ \rightarrow COD^+ + O \quad (8)$$

Thus, reaction 8 is analogous to reaction 7 with different products at a different dissociation limit. The same interpretation holds for the data at 0.85 eV, although at this energy, we do not have the underlying information on the precursor $CO_2D^+$.

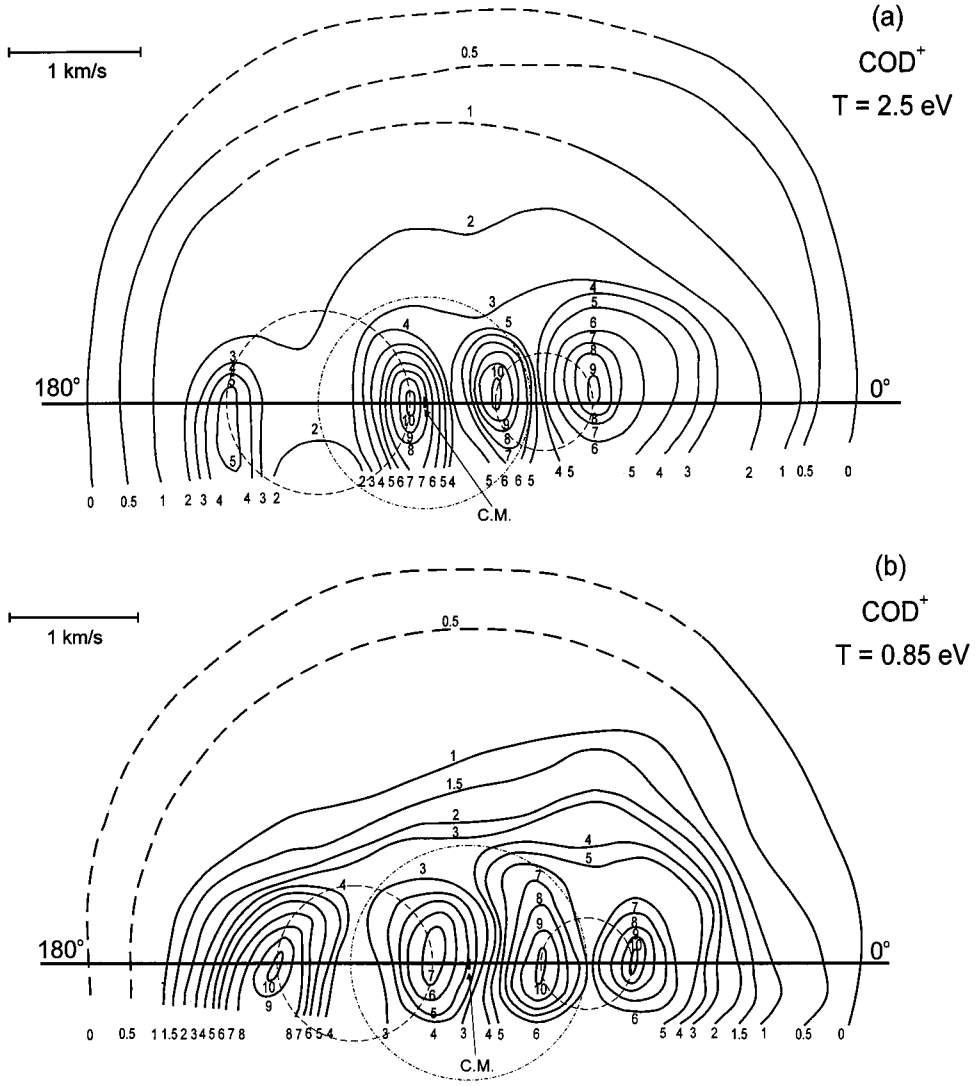


**Figure 8.** Contour scattering diagrams of $COD^+$ at collision energies of (a) 2.5 and (b) 0.78 eV. Designations are analogous to those used in Figure 4. The dash-dotted circle in Figure 8a at $u(COD^+) = 0.8$ km/s and the two dotted circles refer to the discussion of $COD^+$ formation from $CO_2D^+$ (section 3.2.3).

From the separation of the ridges in the pairs of forward and backward peaks in Figure 8, one can conclude that the mean energy released in the dissociation process to $COD^+ + O$ is about 0.1−0.2 eV. The relative cross sections in Figure 1 imply that most of the primary chemical product $CO_2D^+$ dissociates to $COD^+$.

*3.2.4. Formation of $CO^+$.* Formation of the product $CO^+$ was observed both in collisions with $D_2$ and in spontaneous dissociations of the projectile $CO_2^{2+}$ (without gas in the crossed beam).

Figure 9a shows a velocity profile of the $CO^+$ formed in $CO_2^{2+} + D_2$ collisions at 2.48 eV and a laboratory scattering angle of +1.5°. The product is preferentially scattered forward with respect to the C.M. and shows a rather broad distribution that peaks at the laboratory energy of 11.7 km/s [the respective C.M. velocity, $u(CO^+)$, is 0.94 km/s].

One can imagine several processes in which $CO^+$ can be formed: (1) a chemical reaction leading to $CO^+$ and $D_2O^+$; (2) dissociation of the charge-transfer product $CO_2^+$ to $CO^+ + O$, for which the energy release would be close to that expected for the formation of the $CO_2^+ + D_2^+$ pair (assuming small or negligible energy release in the dissociation to $CO^+ + O$); and (3) collision-induced dissociation of $CO_2^{2+}$ on $D_2$ to $CO^+ + O^+$, in which case the translational energy release would be determined by the energy difference between the top of the potential energy barrier for the $CO_2^{2+}$ dissociation and the energy of the $CO^+ + O^+$ asymptote (5.1−5.7 eV; also see later).

In Figure 9b, the velocity profile of $CO^+$ from Figure 9a is plotted as the translational energy profile, assuming either formation of the pair $CO^+ + D_2O^+$ [$T_1'(CO-D_2O)$] or the charge-transfer process [$T_2'(CO_2-D_2)$] and further dissociation of $CO_2^+$ to $CO^+ + O$. It can be seen that the distribution peaks for the former case at an unrealistically small relative translational energy of 0.5 eV, whereas for the latter case, it peaks in the vicinity of about 4 eV. This is the translational energy release expected for the formation of the charge-transfer product $CO_2^+$-($C^2\Sigma^+_g$) (see also Figures 6a and 7a) and its subsequent dissociation to $CO^+(X^2\Sigma^+)$ and neutral $O(^3P)$.

Another possibility is $CO^+$ formation in a collision-induced dissociation of the dication $CO_2^{2+}$ on $D_2$, leading to the formation of the ion pair $CO^+ + O^+$. Because of the difference in the masses of the colliding particles, the change of the C.M. velocity of $CO_2^{2+}$ because of inelastic energy transfer should be small, especially if the projectile ion was formed with considerable vibrational excitation. The origin of the product ion pair formation will then be close to the tip of the laboratory velocity vector of $CO_2^{2+}$, $v(CO_2^{2+}) = 11.22$ km/s (Figure 9a). In the velocity distribution of $CO^+$, the hump in the backward

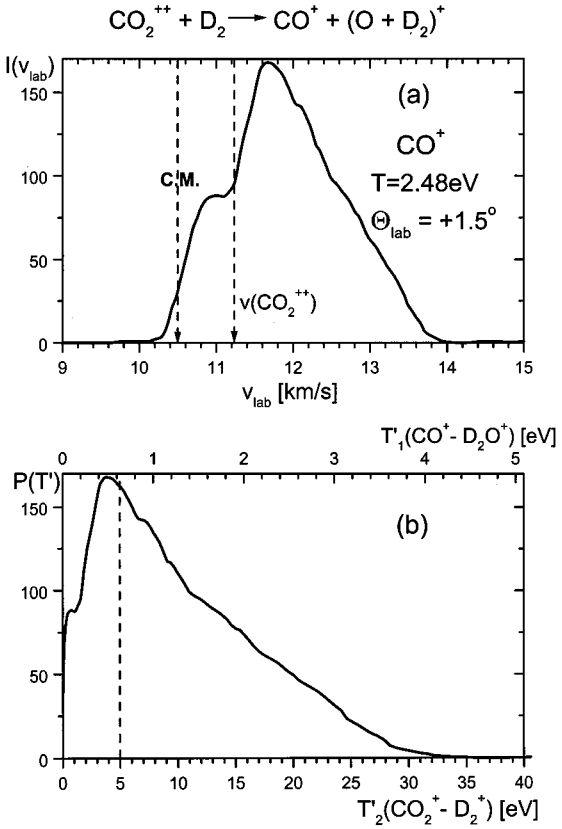


**Figure 9.** (a) Laboratory velocity profile of $CO^+$ formed in $CO_2^{2+}$ + $D_2$ collisions at 2.48 eV and a laboratory scattering angle of +1.5 eV. The vertical dashed lines denote the velocity of the center-of-mass (C.M.) and the laboratory velocity of the reactant ion [$v(CO_2^{2+})$]. (b) Relative translational energy profiles of $CO^+$, $P(T')$, from data in Figure 9a plotted against relative translational energy of the product pairs $CO^+$ + $D_2O^+$ (upper scale) and $CO_2^+$ + $D_2^+$ (lower scale). The vertical dashed line indicates $T_2'$ for the production of $CO_2^+(C^2\Sigma_g^+)$.

direction with respect to $v(CO_2^{2+})$, at 11.0 km/s, corresponds to a relative energy release of the pair $CO^+ + O^+$ of 0.08 eV, and the distribution extends to 0.55 eV. In the forward direction, the peak at 11.7 km/s corresponds to a relative translational energy release of 0.36 eV and extends to about 2.3 eV (velocity of 13.8 km/s in Figure 9a). This value is, however, much too small, as passage over the barrier to the dissociation products $CO^+ + O^+$ should result in a relative energy release of the ion pair of 5.1−5.6 eV (see spontaneous dissociation of $CO_2^{2+}$ below and barrier heights 1, 2, and 3 in Figure 10b).

We conclude, therefore, that the main channel of $CO^+$ formation in $CO_2^{2+} + D_2$ collisions is charge transfer to $CO_2^+(C^2\Sigma^+_g)$ and a subsequent decomposition of this predissociative state[9,21] according to the reaction sequence

$$CO_2^{2+} + D_2 \rightarrow (D_2^+) + CO_2^+(C^2\Sigma^+_g) \rightarrow CO^+(X^2\Sigma^+) + O(^3P) \quad (9)$$

A spontaneous dissociation of $CO_2^{2+}$ was also observed, in the absence of any collision gas in the crossed beam. The registered products were $CO^+$ and also $O^+$. Laboratory energy profiles of both of these ions were measured at the $CO_2^+$ laboratory energies of 6.2 and 10.6 eV, transformed into the velocity profiles, and related to the C.M. of the dissociating pair $CO^+ + O^+$. The velocity profiles at $E(CO_2^{2+}) = 6.2$ eV are given in Figure 10a. The positions of the peaks correspond to a translational energy release of 5.46 eV for $CO^+$ and 5.49 eV for $O^+$, in good agreement. Unfortunately, these values

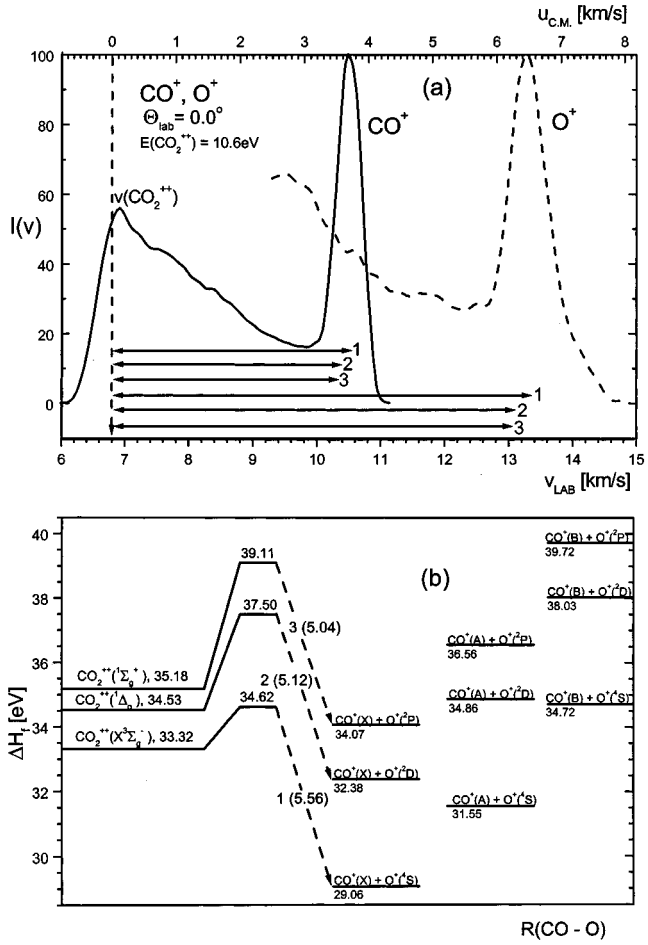


**Figure 10.** (a) Laboratory velocity profiles of $CO^+$ and $O^+$ from spontaneous dissociation of the reactant ion $CO_2^{2+}$ at a laboratory scattering angle of 0.0° and laboratory energy of 10.6 eV. The vertical dashed line shows the laboratory velocity of the reactant ion; horizontal arrows show expected relative translational energies of $CO^+$ and $O^+$, for dissociation processes, as summarized in Figure 10b (numbers 1, 2, and 3 refer to the respective barrier heights). (b) Energetics and translational energy release in the dissociation of ground and excited states of $CO_2^{2+}$. Energy data from ref 17. Numbers in parentheses at barriers 1, 2, and 3 refer to barrier heights.

cannot be used in determining the state-to-state dissociation processes, as the barriers for several processes lead to a comparable energy release[17] and the differences were beyond the energy resolution of this experiment. The data on the barrier heights and dissociation asymptotes of the respective states of $CO_2^{2+}$, as reported in ref 17, are summarized in Figure 10b. The expected product energies are shown by horizontal bars 1, 2, and 3 in Figure 10a.

**3.3. Potential Energy Surface of the System $CO_2H_2^{2+}$.** Calculated stationary points on the potential energy hypersurface of $CO_2H_2^{2+}$ are given in Figure 11. Only triplet states, related to the ground state of the reactant ion are shown. The numbers at the stationary points are calculated values; tabulated thermodynamic values,[24] if used, are given in parentheses. The left side refers to the energetics of reactants and charge-transfer products $[CO_2 + H_2]^{2+}$, the central part to intermediates $[CO_2H_2]^{2+}$, and the central right-hand side to chemical-bond-rearrangement products $[CO_2H+ H]^{2+}$; the extreme right provides relevant data on dissociation products.

The calculated data provide an important source of information for justifying the conclusions drawn from the experimental results. In the reactant valley, the ground-state reactants, approaching on a triplet dication surface, pass through several

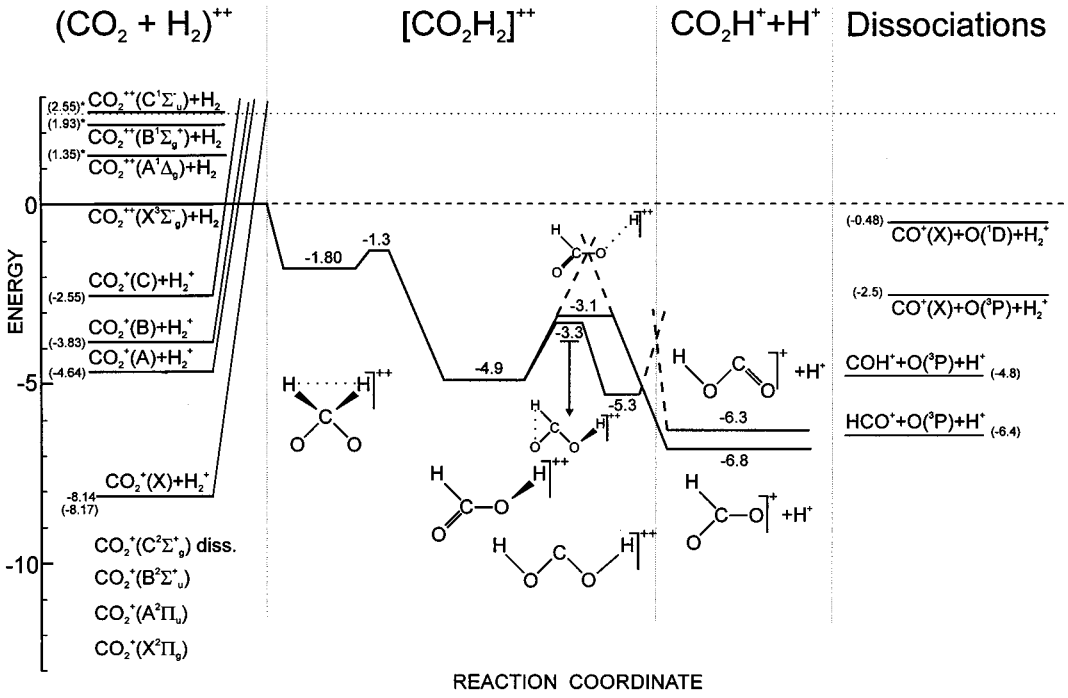


**Figure 11.** Stationary points on the potential energy surface of $[CO_2D_2]^{2+}$ (triplets). Numbers refer to the calculated values of energies of the species, intermediates, and transition states of given structures (tabulated values in parentheses). Horizontal dotted line at 2.5 eV indicates the total energy content of the system at this collision energy.

crossings with Coulomb repulsion hypersurfaces correlating with the charge-transfer products $CO_2^+ + H_2^+$. Excited states $CO_2^+$(A) and $CO_2^+$(B) of the product ion are populated with the highest probability. The energetics for these processes fit the reaction-window model[4] and, thus, confirm again that the model can be applied, at least approximately, even to more complicated molecular systems. Only those collision systems that pass through these crossings can reach small interparticle separations, where intermediates $[CO_2H_2]^{2+}$ can be formed. Intermediates of various structures are more stable, with respect to the reactants, by $-1.8$ to $-5.3$ eV. From an important intermediate structure at $-4.9$ eV, two isomeric branches develop, the H−O-bonded and the H−C-bonded structures. The H−C-bonded structure leads over a barrier to the somewhat more stable product pair $HCO_2^+ + H^+$; an extension of the O−H bond in this structure leads to an initial increase of energy and then, beyond about 2.4 A, to its decrease and the formation of the pair of singly charged ions. Thus, the barrier at $-3.1$ eV can be regarded as resulting from the crossing of the dication potential energy surface with the Coulomb repulsion surface of the two cations $HCO_2^+ + H^+$. We believe that this is the main channel leading from the ground-state reactants on the triplet surface to the chemical-rearrangement products, observed in the experiments as the channel of $DCO_2^+ + D^+$ formation with the high translational energy release via an osculating intermediate with a mean lifetime comparable to about an average rotational period of the intermediate (estimated from the moment of inertia to be about 1.5 ps). Indeed, RRKM calculations (using the vibrational frequencies calculated for the transition state at $-3.1$ eV) show that, at the collision energy of 2.5 eV, the estimated mean lifetime of such an intermediate is about 0.8 ps, in reasonable agreement with the estimations from the experiments. The translational energy release connected with the decomposition of the intermediate can be regarded, in the simplest way, as the statistical translational energy release connected with the decomposition of the intermediate from the well depth with a total energy of $T + E(DCO_2D) = 2.5 + 4.9 = 7.4$ eV, increased by the translational energy release of $-3.1-6.8 = 3.7$ eV connected with sliding from the transition state to the products. Thus, one can expect peaking of the $P(T') - T'$ distributions at about 3.8−4 eV, in general accord with the experimental result in Figure 3 (despite the scatter of experimental data). Further dissociation of the chemical product $DCO_2^+$ presumably goes to $COD^+ + O(^3P)$, with the asymptote lying close by, at $-6.4$ eV.

The formation of a small amount of $CO_2^+$ by further dissociation of the bond-rearrangement product $CO_2D^+$ (reaction 7) may be connected with the formation of an excited state of this product in a process of low translational energy release; the primary product then dissociates further to an excited state of $CO_2^+$. However, we cannot exclude the possibility that this process, of a very small relative weight, is connected with reactions of an excited (singlet) reactant $CO_2^{2+}$, and thus, any further attempt to discuss details of its formation would be purely speculative.

## 4. Conclusions

(1) Chemical reactions and charge-transfer processes in the system $CO_2^{2+} + D_2$ were investigated in a series of crossed-beam scattering experiments. The main heavy products identified were the singly charged ions $CO_2^+$, $CO_2D^+$, $COD^+$, and $CO^+$.

(2) The relative total cross sections of the most important products are approximately in the ratio $CO_2^+$:$COD^+$:$CO_2D^+$ = 100:10:1 and show only a slight dependence on the collision energy over the measured range, 0.5−4 eV (C.M.).

(3) $CO_2D^+$ was formed in two processes of different translational energy release in a nondissociative chemical reaction leading to the two singly charged ions $CO_2D^+ + D^+$; both processes involved formation of an intermediate $(CO_2D_2)^{2+}$.

(4) $CO_2^+$ is formed predominantly in the A and B excited states by a nondissociative charge-transfer reaction; a small amount of the product (2−4%) is formed by subsequent dissociation of the singly charged chemical product $CO_2D^+$

(presumably formed in an excited state) to $CO_2^+$ and neutral D with an average relative energy release in the dissociation of about 0.2−0.3 eV.

(5) $COD^+$ results from a subsequent dissociation of the singly charged chemical product $CO_2D^+$ (formed in the high translational energy release channel) to $COD^+ + O$.

(6) $CO^+$ comes from two different processes: (a) dissociation of the charge-transfer product $CO_2^+$, most likely formed in the predissociative state $C^2\Sigma_g^+$, via $CO_2^+(C^2\Sigma_g^+) \rightarrow CO^+(X^2\Sigma^+) + O(^3P)$ and (b) spontaneous dissociation of the reactant ion $CO_2^{2+}$, vibrationally excited in its formation to the dissociation barrier. The specific state-to-state assignment is difficult, as the predissociation processes of the ground and excited states of $CO_2^{2+}$ lead to very similar translational energy releases.

(7) Calculated stationary points on the hypersurface $(CO_2H_2)^{2+}$ helped to justify the conclusions of the experimental study, to assign probable structures of the intermediates and the products, and to better understand the dynamics of the observed reactions.

**Acknowledgment.** Partial support of this research by Grants 203/97/0351 and 203/00/0632 of the Grant Agency of the Czech Republic is gratefully acknowledged. The study is a part of the European Network RTN1-1999-00254 "Generation, Stability and Reaction Dynamics of Multiply Charged Ions" (MCInet).

## References and Notes

(1) Weisshaar, J. C. *Acc. Chem. Res.* **1993**, *26*, 231.
(2) Price, S. D.; Manning, M.; Leone, S. R. *J. Am. Chem. Soc.* **1994**, *116*, 8673.
(3) Herman, Z. *Int. Rev. Phys. Chem.* **1996**, *15*, 299.
(4) Dolejšek, Z.; Fárník, M.; Herman, Z. *Chem. Phys. Lett.* **1995**, *235*, 99.
(5) Herman, Z.; Žabka, J.; Dolejšek, Z.; Fárník, M. *Int. J. Mass Spectrom.* **1999**, *192*, 191.
(6) Newson, K. A.; Price, S. D. *Chem. Phys. Lett.* **1997**, *269*, 93.
(7) Mathur, D. *Phys. Rep.* **1993**, *225*, 193.
(8) Ehbrecht, A.; Mustafa, N.; Ottinger, Ch.; Herman, Z. *J. Chem. Phys.* **1996**, *105*, 9833.
(9) Price, S. D.; Rogers, S. A.; Leone, S. R. *J. Chem. Phys.* **1993**, *98*, 9455.
(10) Koyano, I. Himeji Institute of Technology, Himeji, Japan. Private communication, 1999.
(11) Friedrich, B.; Herman, Z. *Collect. Czech. Chem. Commun.* **1984**, *49*, 570.
(12) Frisch, M. J.; Trucks G. W.; Schlegel; H. B.; Scuseria; G. E.; Robb, M. A.; Cheeseman, J. R.; Zakrzewski, V. G.; Montgomery, J. A., Jr.; Stratmann, R. E.; Burant, J. C.; Dapprich, S.; Millam, J. M.; Daniels, A. D.; Kudin, K. N.; Strain, M. C.; Farkas, O.; Tomasi, J.; Barone, V.; Cossi, M.; Cammi, R.; Mennucci, B.; Pomelli, C.; Adamo, C.; Clifford, S.;. Ochterski, J.; Petersson, G. A.; Ayala, P. Y.; Cui, Q.; Morokuma, K.; Malick, D. K.; Rabuck, A. D.; Raghavachari, K.; Foresman, J. B.; Cioslowski, J.; Ortiz, J. V.; Stefanov, B. B.; Liu, G.; Liashenko, A.; Piskorz, P.; Komaromi, I.; Gomperts, R.; Martin, R. L.; Fox, D. J.; Keith, T.; Al-Laham, M. A.; Peng, C. Y.; Nanayakkara, A.; Gonzalez, C.; Challacombe, M.; Gill, P. M. W.; Johnson, B G..; Chen, W.; Wong, M. W.; Andres, J. L.; Head-Gordon, M.; Replogle, E. S.; Pople, J. A. *Gaussian 98*, revision A.6; Gaussian, Inc.: Pittsburgh, PA, 1998.
(13) Becke, A. D. *J. Chem. Phys.* **1993**, *98*, 1372 and 5648.
(14) Becke, A. D. *J. Chem. Phys.* **1986**, *84*, 4524.
(15) Millie, P.; Nenner, I.; Archirel, P.; Lablanquie, P.; Fournier, P.; Eland, J. H. D. *J. Chem. Phys.* **1986**, *84*, 1259.
(16) Penent, E.; Lablanquie, P.; Hall, R. I.; Ahmad, M.; Diehl, S.; Kjeldsen, H.; Eland, J. H. D.; Ito, K.; Hikosaka, Y.; Muehleisen, A.; Pelicot, P.; Smit, Z.; Zitnik, M.; Koike, F. *XXI International Conference on the Physics of Electronic and Atomic Collisions*, Sendai, Japan, July 20−27, 1999; Book of Abstracts, p 50.
(17) Hochlauf, M.; Bennett, F. R.; Chambaud, G.; Rosmus, P. *J. Phys. B: At., Mol. Opt. Phys.* **1998**, *31*, 2163.
(18) Jonathan, P.; Hamdan, M.; Brenton, A. G.; Willett, G. S. *Chem. Phys.* **1988**, *119*, 159.
(19) Mrázek, L.; Žabka, J.; Herman, Z. Unpublished results.
(20) Potts, A. W.; Williams, T. A. *J. Electron Spectrosc. Relat. Phenom.* **1974**, *3*, 3.
(21) Eland, J. H. D.; Berkowitz, J. *J. Chem. Phys.* **1977**, *67*, 2782.
(22) Eland, J. H. D. *Int. J. Mass Spectrom. Ion Processes* **1973**, *12*, 397.
(23) Friedrich, B.; Pick, S.; Hládek, L.; Herman, Z.; Nikitin, E. E.; Reznikov, A. I., Umanskij, S. Ya. *J. Chem. Phys.* **1986**, *84*, 807.
(24) Rosenstock, H. M.; Draxl, K.; Steiner, B. W.; Herron, J. T. *J. Phys. Chem. Ref. Data* **1977**, *6*; Supplement No. 1.